

MINERvA neutrino detector response measured with test beam data

MINERvA Collaboration

MINERvA Addresses placeholder in template

Abstract

The MINERvA collaboration operated a MINERvA-like detector in a hadron test beam at the Fermilab Test Beam Facility, experiment number T977. This article reports measurements with samples of protons and pions and electrons, from which calibrations of Birks' constant, calorimetry, and a test of proton tracking efficiency are obtained. These results are used to tune the MINERvA detector simulation and evaluate systematic uncertainties in support of the MINERvA neutrino cross section measurement program.

Keywords: `elsarticle.cls`, L^AT_EX, Elsevier, template

2010 MSC: 00-01, 99-00

Note to MINERvA reviewers

This list will allow for quick location of additional information and supporting plots from our tech notes, and will be removed before being submitted to NIM.

- 5 Test beam beamline resolution and systematic errors
 - Devan and Gran, TN017, docdb:8547
 - Test beam detector calibrations, Gran et al., TN018 docdb:8686
 - Pion reaction cross section, Higuera, TN033 docdb:9031
 - Birks' law parameter from MINERvA testbeam data, Gran, TN037 docdb:9131
- 10 Test beam pion calorimetry, Gran, TN045 docdb:9474
 - Electron calorimetry and the e/π ratio, Bergan, (no TN#) docdb:9929
 - Test beam proton calorimetry, Devan, TN051 docdb:9986
 - Short track reconstruction efficiencies using test beam protons,
 - McGivern, TN048, docdb:10367

15 **1. Introduction and test beam goals**

The MINERvA experiment[1] is designed to make measurements of neutrino nucleus cross sections with high precision. An important part of these [2, 3, 4, 5, 6] and future cross section measurements is the estimate of the energy of one or more hadrons exiting the nucleus. These are moderate energy recoil nucleons, especially protons and pions from inelastic production, or soft nucleons and nuclear fragments. This test beam experiment is designed to validate the Monte Carlo simulation of the detector response to these particles. Significant results presented in this paper include a measurement of the Birks' law parameter, constraints on proton, pion, and electron calorimetry, and a study of tracking efficiency for protons.

The detector used to take these data was built to be identical in most respects to the MINERvA detector installed in the NuMI neutrino beam at Fermilab. This test beam detector was placed in a new hadron beamline at the Fermilab Test Beam Facility (FTBF) for a data run in summer 2010. Differences between the two designs do not impact the analysis, rather they mitigate special aspects of the beam environment in FTBF and allow for a data set better focused on the Birks and calorimetry results.

The energy range covered by these data is well matched to the energy range of protons and pions and EM showers in the MINERvA low energy neutrino and anti-neutrino data, taken from 2010 to 2013. This is especially true for the reactions from quasi-elastic scattering through Δ and other resonance production at lower invariant mass; each is a pillar of the MINERvA neutrino physics program. These energies also cover the lower part of the range expected from hadrons produced in neutrino deep inelastic scattering.

40 **2. Fermilab Test Beam Facility tertiary hadron beam**

This beam was built for the MINERvA experiment in partnership with the Fermilab Test Beam Facility. It is produced from 16 GeV pions colliding with a copper target with all species exiting a collimator at an angle of 16 ± 1

degrees. With the large detector aperture (described later) and our chosen
45 beam tune, the beam delivers a broad distribution of protons and pions from
0.35 to 3.0 GeV/c that are species and momentum tagged on a particle by
particle basis. The usable momentum range for these analyses is 0.35 to 2.0
GeV/c which provides roughly ten thousand particles each of proton, π^+ , and
 π^- , enough that these measurements are systematics dominated. The electron
50 content of the beam is small and limited to low momentum, but has enough
events for analysis. In addition, there is a 5% component of kaons, plus smaller
components of deuterons and alpha particles which are not part of the results
presented here.

The species and momentum is tagged particle by particle using time of flight
55 (TOF) and position measurements from four wire chambers (WC). The resulting
distribution is shown in Fig. 1 after quality cuts for well-measured particles. The
pion, kaon, proton, and deuteron/alpha components are clearly seen, along with
low momentum electrons near 20ns. There is also accidental background near
40 ns when another particle coincidentally passes through the TOF separated
60 by one 19 ns spacing of the beam. The momentum estimate uses a detailed map
calculated using finite element analysis software from the specifications for the
two dipole magnet coils and steel and the position survey of their placement
relative to each other. The central value of the magnetic field is scaled down
to match the measured field of the magnet which is known to better than 0.5%
65 precision. The longitude and transverse measurements of the field are well
described by the calculated field and how accurately they are modeled is the
basis for estimating the uncertainty in the momentum. The other uncertainty
comes from the accuracy of the position survey of the four wire chambers. In
total, the bias uncertainty on the momentum assignment ranges from 1% at low
70 energy to 2% at higher energy.

The iterative fit uses a stepper within the non-uniform calculated field to
estimate the field integral, and a Kalman Filter technique is used to obtain
the momentum and its uncertainty for each trigger. Resolution is evaluated
particle by particle and is 2.5% for pions and ranges from 5% to 3% for protons;

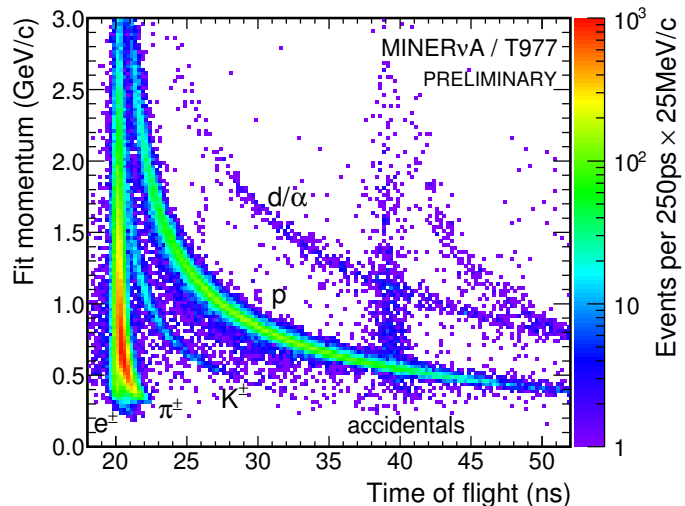


Figure 1: The measured momentum and time of flight used to separate different particle species and backgrounds.

75 it is driven by multiple scattering at low momenta and by the wire pitch and beamline length at high momenta. This feature of the beamline is modeled accurately enough and is not a limiting factor for these analyses. The resolution on the time of flight of 200 ps limit the ability to separate electrons from pions and is a source of uncertainty for that measurement.

80 3. MINERvA test beam detector and calibration

The detector exposed to the FTBF beam (hereafter called the test beam detector) is a miniature version of the full MINERvA detector installed in the NuMI neutrino beam. It is made of forty rectangular planes of scintillator with length 1.07 meters and 63 strips wide, in contrast to a hexagon shape made
85 of 124 planes of 127 strips in the central tracker region followed by another 20 planes each of ECAL and HCAL in the full MINERvA detector. Both detectors share the same three-view UXVX sequence of planes with U and V rotated ± 60 degrees, which allowing for dual stereo reconstruction of multiple tracks for the full MINERvA and very good reconstruction of single tracks in the test beam

90 detector.

The signal chain from scintillator to wavelength shifting (WLS) fiber to PMT to digitization is the almost identical. The exception is the test beam detector has no clear fiber, the WLS fiber connects directly to the PMT a half-meter out of the plane. The effect of smaller scintillator planes and no clear fiber is that the
95 test beam detector has about 50% higher light yield, and corresponding better resolution for some kinds of measurements, compared to the full MINERvA.

Unlike the MINERvA detector which reads out every plane on the same side, the test beam detector alternates readout in groups of four planes, one UXVX set rotated 180 degrees. Mechanically this allows the planes to be placed
100 closer together, with an air gap only slightly larger than the MINERvA detector. Because the beam bend magnets steer different momentum particles to different portions of the detector (and at different angles) this mitigates a few-percent momentum dependent bias uncertainty that would come from this geometry correlated with the position dependent optical attenuation.

105 The detector energy scale is calibrated using the same strategy as the MINERvA detector installed in the NuMI neutrino beam, and is described in [1]. There are a few variations to note. The absolute response calibration is carried out with broad spectrum cosmic ray muons (and a simulated spectrum) rather than momentum-analyzed muons from the NuMI beam. The energy scale calibration using these muons allows us to tune the uniformity between scintillator
110 strips, simulate the right photon statistics from energy deposits, and get the absolute energy scale calibration. These calibrations do not include energy that appears off the muon track due from cross talk a features treated separately in the analysis described in this paper. Secondly, temperature dependence is
115 more important than it is in the NuMI hall. The overnight cosmic muon sample spans the same range of temperature as the daytime hadron sample. The detector response is corrected for that dependence and a residual uncertainty is included with the systematic errors.

Unlike the MINERvA detector, the test beam detector has removable ab-
120 sorber. We took exposures of two configurations: one with 20 planes with 1.99

mm thick Pb absorber (ECAL) and 20 planes with 26.0 mm thick Fe absorber (HCAL), and one with 20 planes with no absorber (tracker) and 20 planes of ECAL. For compactness, this document will refer to these configurations as EH and TE respectively. This covers the main downstream regions of the MIN-
 125 ERvA detector, which has 124 planes of tracker followed by 20 ECAL and 20 HCAL.

4. Data sample and simulation

For the EH configuration, the following figures show the energy spectra for π^+ , π^- , and protons.

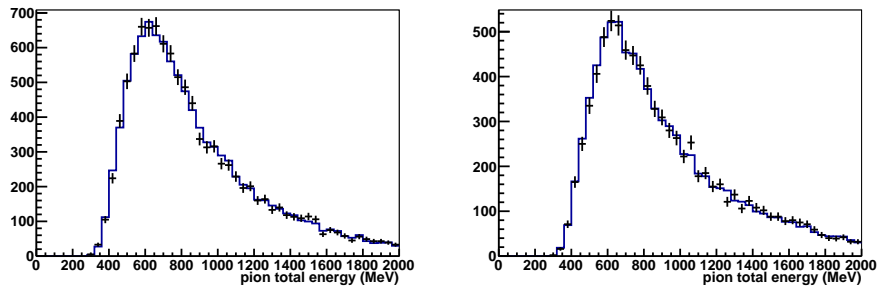


Figure 2: Measured spectra for π^- , π^+ , and proton samples, after selection. The blue histogram is taken from a MC simulation that was seeded with measured particle momenta and trajectories from the data. [ADD PROTON EH PLOT, maybe only show one pion plot as an example.]

130 In the analyses considered in this manuscript, the data are compared to a full, high statistics simulation. The spectrum for the simulation are the actual data particles' position and momentum at WC3, smeared according to the estimated resolution on a particle by particle basis, and then propagated through a simulation of the material of WC3, WC4, the downstream TOF, the cosmic
 135 muon trigger scintillator, and into the detector. Using the estimated resolution for each particle and a Gaussian smearing allows us to use the same data particles multiple times and generate large MC samples, typically 20 to 40 times.

We observe that the MC reproduces the data for the special situations where the beamline resolution dominates, such as for protons that stop at the end of their range, validating that the beamline characteristics are well simulated.

The MC does not simulate any beamline pileup effects, either from particles that are exactly in-time (from the same parent 16 GeV pion hitting the target) or secondaries from another pion in an nearby 19 ns slot in the Fermilab Main Injector 52 MHz accelerator structure. Because we collect data for 16 microseconds around each trigger, and because some incident triggers should spatially leave much of the detector quiet, the data itself contains a record of the average pileup background around valid triggers. We make a statistical subtraction and evaluate an uncertainty. These estimates were validated, and some cleaning selections were developed using the totally awesome web-based MINERvA event display [7], in many cases with the help of undergraduate research assistants.

The basis of the simulation uses Geant4 version 9.4p2 [8, 9] and our best description of the detector geometry and material. The scintillator plane is made of 1.801 g/cm² of plastic scintillator, WLS fiber, and the co-extruded TiO₂ reflective coating. Added to this is another 0.226 g/cm² of epoxy and Lexan. In the ECAL portion of the detector there are planes of Pb with thickness 2.30 g/cm² and in the HCAL version there is 20.4 g/cm² material that is 99% Fe and 1% Mn. The Pb and Fe absorber are similar to the MINERvA detector, but we use the as-measured test beam detector quantities in the simulation and to evaluate material assay uncertainties. The scintillator strips were made at the same facilities immediately following the production of MINERvA planes, and the manufacturing modifications for smaller planes make negligible difference.

Almost all aspects of the detector response are simulated using details constrained by calibration data and bench tests, including the Birks' law parameter measured from these data, described below. A few features are not simulated, of which PMT after-pulsing is the only significant omission requiring careful treatment. All uncertainties in this category that significantly affect the analysis are described later.

5. Birks' Law parameter

With a well calibrated beam and detector, the test beam data are used to
170 obtain a measurement of the Birks' Law parameter for our scintillator. The
scintillator is made of polystyrene doped with 1% PPO and 0.03% POPOP by
weight [1]. Birks' Law describes the quenching effect where the conversion of
energy to scintillation photons is suppressed for high, localized dE/dx . This
is especially important at the end of proton tracks in neutrino analyses, which
175 why we need this calibration and test beam protons are the means to obtain
it. This measurement is done with protons that appear to stop in the upstream
20 tracker planes of the TE detector configuration. This measurement comes
first of the results in this paper, because the correctly adjusted response and its
uncertainty play a role in the calorimetry measurements to follow.

180 A sample of protons that stop at the end of their expected range is selected
from the larger set of good proton events. Protons that appear to stop between
planes 9 and 19 inclusive are checked that their range is consistent with their
incoming energy. It is not done using a simulation; for events that stop in a partic-
ular plane, the end-of-range protons form a distinct peak at the appropriate
185 energy while protons that interact are a high energy tail; we select the former.

Once selected, the incoming energy of the protons (according to the beamline
measurement) is not used for analysis, the dE/dx profile is built backward from
the observed end of each proton track. This is done separately for the data
and MC and is less sensitive to uncertainties or mismodeling of the incoming
190 proton momentum or material assay. On this latter point, we observe that the
proton range is very well modeled by the simulation. The simulated protons
stop 1.1% earlier than the data, which is a smaller discrepancy than the 1%
beamline momentum and 1.4% material assay uncertainties. This cross-check
uses a Gaussian fit to find the end-of-range peak used to select the Birks' sample,
195 and is shown in Fig. 3. Stopping protons are such a high resolution sample, the
widths of those Gaussian fits (10 to 15 MeV, not shown) are primarily driven
by the beamline and multiple scattering resolutions, and are also well described

by the simulation.

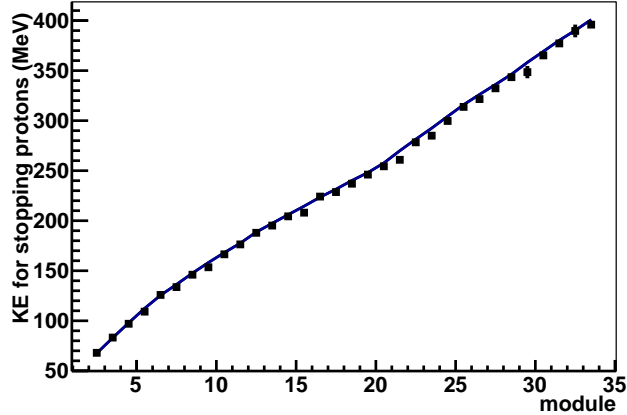


Figure 3: Kinetic energy from a Gaussian fit to the peak energy for protons that appear to stop in each TE plane (module). The MC stops 1.1% earlier than the data, a discrepancy which is smaller than the beamline momentum and material assay uncertainties. Most error bars are less than 1% and are too small to see.

With this selected sample, the activity from each proton is analyzed as a
200 function of how many planes it is from the last plane with activity. The binned
distribution of measured energy in each plane from the end will be used in the
fit, but to ease visualizing the trend, a Gaussian can be fit to the peak and
plotted. Both the binned distribution and the fitted distribution are done for
the data, the default simulation before fitting for a better Birks' parameter,
205 and two alternate simulations with 30% variation in the pre-fit parameter. The
points in this visualization shown in Fig. 4 are from a Gaussian fit, which is a
good approximation for most planes, but because the proton stops at different
depths in the final plane, the distribution is not actually Gaussian. The trend
clearly indicates the original estimate of Birks' parameter needs to be shifted to
210 produce less quenching.

The Birks' parameter is obtained by using the default simulation with a
candidate Birks' parameter and two other simulations with separate \pm Birks'

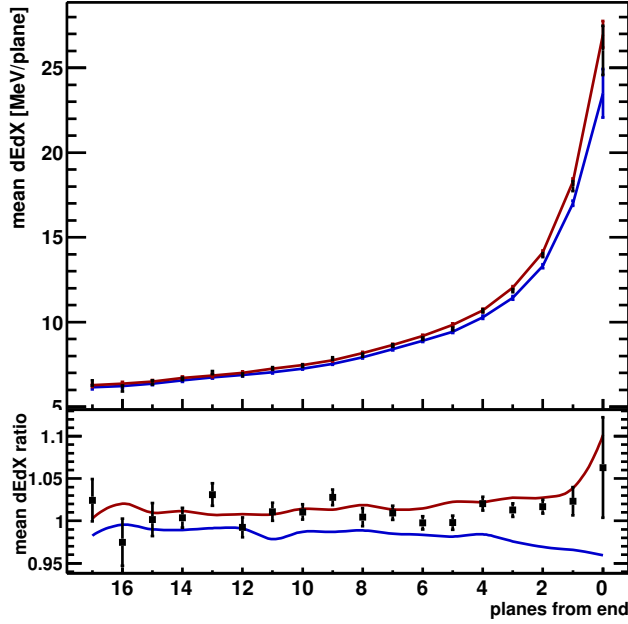


Figure 4: The measured energy deposit per plane for data compared to the simulation with the before-fit Birks' parameter of 0.133 mm/MeV and the original -30% (red) and +30% (blue) limits to the parameter.

parameters, and interpolating to get good agreement with the data. The data
 used for the fit are the inputs to Fig. 4, namely the binned profile of dE/plane for
 215 each plane back from the end of the track. The fit is limited to bins of dE/plane
 where the statistics are good, 123 bins total. In the fit, the overall energy
 scale is an unconstrained parameter, which simultaneously accounts for both
 the energy scale uncertainty and the correlation between the calibrated energy
 scale and Birks' parameter. Also, an amount of dE smearing that accounts
 220 for unsimulated calibration effects was allowed to vary, though it yields the
 same 5.5% result as found for the full MINERvA. Thus the fit is done using a
 parameter scan in this 3D parameter space of Birks' parameter, energy scale,
 and smearing of reconstructed energy deposits. The procedure is iterated and
 reliably converges.

225 The best value for the Birks' parameter is 0.0905 ± 0.015 mm/MeV. This
value is near the -1σ limit of the ab-initio estimate used by MINERvA for analy-
ses through 2014, confirming that Birks' effect uncertainties in prior publications
are accounted for, and future simulations using new value have an uncertainty
half the size of the old value. The best fit describes the data well, yielding a
230 χ^2 of 124 for 120 degrees of freedom.

This is a systematics dominated measurement. The main systematic comes
from the fit and the correlation with the energy scale, with similar size system-
atics from uncertainties in the material assay and the response variation among
the limited set of physical planes being tested.

235 Because this parameter is obtained by matching the MC simulation to data,
it might be considered an effective parameter. In addition to energy scale cor-
relations and Birks' quenching, it is accounting for the accuracy of the Geant4
energy loss simulation and our choice to use the default (adaptive) Geant4 step
size, in addition to the actual Birks' quenching effect. A more coarse aggre-
240 gation of Geant4 steps at the scale of one scintillator bar yields an increase in
the response of about 4% in the last plane and a slightly better $\chi^2 = 118$; the
typical dx has increased, so dE/dx has decreased, so there is less Birks' suppres-
sion. Such an extreme effect would cause a bias in the fit Birks' parameter of
0.008 (about half the total uncertainty). However, this particular measurement
245 is specifically matched to the Geant4 and hit aggregator settings that are used
by the full MINERvA simulation as of late 2014, so this is a cross check and
not an uncertainty.

Another detector response parameter that has systematic effects, especially
on calorimetry, is the nonlinear response of the photo-multiplier tubes due to
250 saturation effects in the dynode current. This non-linearity sets in for high
instantaneous current at the anode, and so is a function of charge measured
by the front end board digitization module. As of this writing, MINERvA does
not have an in-situ measurement under circumstances that are equivalent to real
light in our scintillator bars, but we have a reference non-linearity curve obtained
255 from bench tests. The dE/plane profile in Fig. 4 is distorted by nonlinearity in

ways different from either Birks' parameter or energy scale, so we investigate the size of possible nonlinearity. We find that applying non-linearity of 20% of the reference degrades the χ^2 by one unit, with a correlated shift in Birks' parameter. Since applying some nonlinearity does not give an improvement in the χ^2 , the best fit value is effectively none. This actually means that at 20 MeV per plane, we do not have sensitivity to nonlinearity effects with these data. We use this as an uncertainty in the Birks' parameter measurement, but apply a larger uncertainty of 50% of the reference to account for non-linearity effects when higher energies are deposited in a single strip.

6. Proton calorimetry

This test beam experiment is designed to constrain the uncertainty on the single particle calorimetric response to protons and pions. For low multiplicity neutrino events we reconstruct the hadron response particle by particle using range, calorimetry, or a combination of the two. For high multiplicity hadron systems from neutrino events, the total energy of the hadronic recoil system (everything but the outgoing charged lepton) is summed. In both cases, when the hadron(s) interact, an estimate of the missing energy, energy lost to unbinding nucleons and to neutral particles, is used to correct the observed response and obtain an unbiased estimator for the hadron system. In all cases, a major ingredient is the MC prediction for the single particle response, which is constrained with these data.

The hadron event is reconstructed by summing the calibrated energy measured in the scintillator. The standard tracking algorithm is applied to each event. If a track segment is found, the 3D location of hits on the track are known and used to make a correction for attenuation in the scintillator strip to the point where the particle passed. For all hits not on tracks, the attenuation estimate is made to the center of the strip. Then a correction for the passive material fraction for each plane is applied; a factor of 1.255 in the tracker, 2.077 in the ECAL, and 10.727 in the HCAL. Because the MEU tuning does not in-

285 clude cross talk in the energy scale, but it is proportional to the total of the
energy deposits, the measured cross talk fraction of 4.2% is subtracted from
both data and MC. Unlike the typical MINERvA neutrino analysis, the test
beam analysis sums over the entire digitized event, rather than a window from
-20 ns to +35 ns around the peak in the cluster timing distribution. The latter
290 technique is tested as a cross check.

There is a background due to pileup in the beamline. In the EH detector
configuration, it is reduced by using activity in the last four planes as a veto. The
remaining background has been estimated two ways, by inspecting activity 30
ns earlier than the triggered particle and for the lowest energy proton sample by
295 inspecting activity deep in the detector where there should be negligible activity.
When extrapolating these methods in time and space, they both yield the same
4 MeV per event on average, though it actually arrives in the form of fewer but
larger energy deposits. For the mean response, this is simply subtracted. At
higher energy, the use of the veto leads to another bias of about 1% estimated
300 using the MC, because real hadron interactions put energy into those planes.
This bias is repaired with an energy dependent correction.

The corrected estimate for the energy is compared to the available energy,
which is just the kinetic energy for the proton. This is done event by event. Then
the events are binned by energy, from which we compute the mean and RMS
305 for each bin. The results for the mean are plotted in Fig. 5. The error band
on the MC represents the total systematic uncertainty. The proton response
has several features in this energy range. At low energy, the probability for a
proton interaction is low. The result is that most of the energy is measured for
most of the protons, and the distribution of response is approximately Gaussian
310 around this mean. At 0.3 GeV, the protons simultaneously begin to produce Δ
resonances when they interact in nuclei and also penetrate to the HCAL. The
latter leads to a drop in response because Δ production generically leads to lower
response through neutral final states and unbinding of additional nucleons.

The MC tracks the proton response well over the entire range. This is shown
315 in the form of the ratio data/MC for the mean response in each energy bin. The

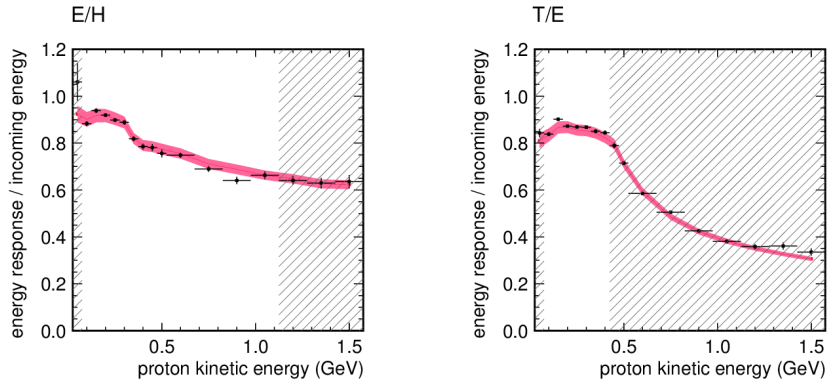


Figure 5: Proton response for EH left and TE right. See text for discussion. [Zoom in on the vertical axis to 0.3 to 1.1 to better show features.]

MC has negligible statistical error, the systematic uncertainty is shown, and the data is shown with statistical uncertainties in Fig. 6. Within the systematic un-

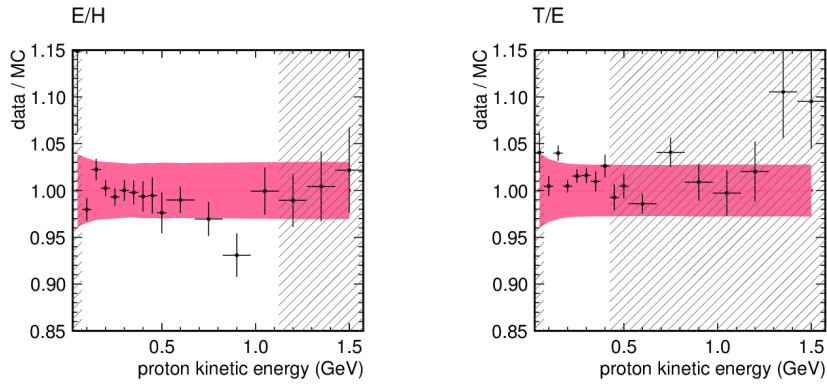


Figure 6: Proton response ratio of data to MC.

certainties, the MC describes the data well. There is mild evidence of systematic effects consistent with any combination of several calibration uncertainties, described in its own section. There is a special pion pileup background at 0.15 GeV in the data because those protons take 19 ns to travel the beamline, the same as the timing of the 53 MHz accelerator structure. It is treated [how cuts

or correction] and can explain the discrepancy in that data point. The data point at 0.9 GeV corresponds to no special features of the experimental setup, and has the character of a $\sim 3\sigma$ fluctuation.

The response at low energy for the TE detector is partly correlated to the tuning of Birks' constant, because up to 0.25 GeV they are the same proton events. However, the strip response energy scale does not come from the free parameter in the Birks' fit. Instead, the calibration muon sample was refit using the measured Birks' parameter to obtain the final strip energy calibration.

In these figures we show the comparison of data and MC in a region at higher energy, which is shaded. At these energies in the TE configuration we are losing containment of charged particles produced in the hadronic interaction, and the calorimetric response no longer represents the kind of result we expect for the full MINERvA detector. Instead, these points demonstrate that the MC is still doing an adequate job describing the data.

In addition to the response, it is important for MINERvA neutrino analyses that we know the fluctuations in the response are well simulated. The basic shape of the distribution of response particle by particle is well described, and the RMS of the distribution is used to quantify the trend and the agreement, as shown in Fig. 7. The statistical uncertainty on the RMS is shown, no systematic uncertainty is quantitatively considered.

At all energies, the MC response has a lower RMS, more prominent at low energy. Though the deviation can be taken to be a conservative uncertainty on the calorimetric resolution, the higher RMS in the data is partly from pileup events from the beamline, which are not expected to have the same magnitude effect for the pion sample, nor the same origin as events in the full MINERvA.

The Δ feature combined with events that are more likely to put energy affects the resolution in the same 0.3 to 0.5 GeV energy range.

Of special interest is the resolution for the lowest energy protons which are contained in the tracker portion of the TE detector configuration. These correspond to the protons typically found at the vertex of a neutrino interaction from quasi-elastic and resonance production and include products of the intranuclear

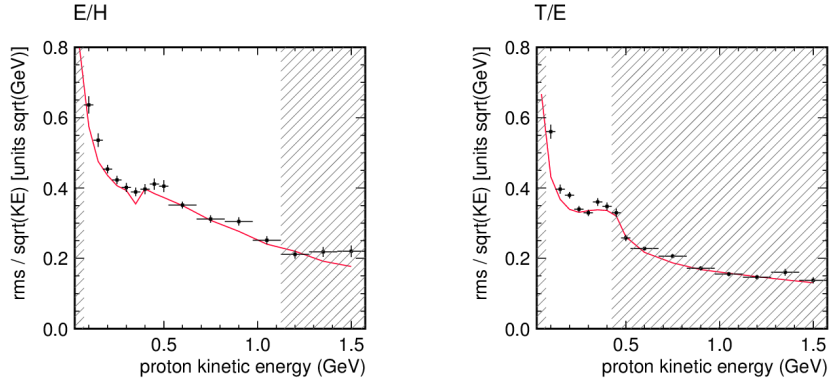


Figure 7: Calorimetric resolution in proton response for the EH configuration (left) and TE (right). [Switch to absolute RMS on the fractional energy response, without the \sqrt{E} .]

rescattering process. In this range a Gaussian fit to the peak gives a resolution
 355 of 18% for protons energetic enough to travel through more than one plane but
 not energetic enough to excite Δ resonances in the nucleus, between 0.05 GeV
 and 0.2 GeV, and comes mostly from fluctuations at the end of the range. Above
 this point Δ production becomes important, reducing the stopping component
 to about half the total, and the distribution from which the RMS is computed
 360 picks up a low-side tail whose shape is well modeled by the MC.

7. Systematics for single particle response

The systematic uncertainties on the single particle response described here
 also apply to the pion measurement that follows with only a few differences.
 These systematic errors are evaluated using a variety of methods. Some are done
 365 by varying the selection criteria for data and MC and evaluating inconsistencies
 in the changed response, others are done comparing a modified MC to the default
 MC, and some are done by dividing the data sample into halves according
 to natural variations in detector and run conditions. The largest sources of
 uncertainty are described here.

source	TE p	EH p	EH π^+	EH π^-
beam momentum	1.9%	1.9%	1.0-2.0%	1.0-2.0%
Birks' parameter	2.0 to 0.9	2.0 to 1.2	1.0	1.0
temperature stability	1.0	1.0	1.0	1.0
PMT nonlinearity	0.7	0.7	0.9	0.9
event selection	<0.2	<0.2	0.7	1.5
energy scale	0.6	0.6	0.6	0.6
cross talk	0.7	0.9	0.5	0.5
beamline mass model	0.7	0.7	<0.2	<0.2
total	3.4 to 2.8%	3.5 to 3.0%	2.6 to 3.4%	2.9 to 3.6%

Table 1: Percent systematic uncertainties on the single particle response for data vs. MC comparison. Additional uncertainties on the energy scale and absorber material apply equally to data and MC absolute response, and are described in the text. The total range represents the evolution with energy from 0.1 to 0.4 GeV for TE protons, 0.1 to 1.0 GeV for EH protons, and 0.4 to 2.0 GeV for both pion samples.

370 7.1. Beam momentum

This uncertainty is intrinsic to the design of the beam and the estimate of the momentum of the incoming particle. An uncertainty here has the trivial effect of shifting the denominator of the fractional response. It comes from the wire chamber survey and the measurement and simulation of the magnetic field. It is highly correlated between neighboring energy bins, but the uncertainty permits some amount [need estimate] of slope from low to high energies. Because it is an uncertainty on the momentum, it translates differently to uncertainties on the available particle energy for protons and pions.

7.2. Birks' parameter

380 Even after producing a best fit Birks' parameter, the remaining improved uncertainty is still one of the largest contributions to the accuracy of the result. Because low energy protons almost always have a high dE/dx activity at the very end of the proton's range, and because that activity is a larger fraction of

the total energy for low energy protons, that sample is most affected by this
385 uncertainty.

7.3. Temperature stability

The response of the detector to cosmic ray muons for the data is calibrated
against the measured temperature as a function of time to account for the
change from day to night and from day to day during the run. This gives a
390 correction which is then applied to energy deposits in the beam data. The
simulation has no temperature dependence. The uncertainty on the accuracy of
that calibration yields a data/MC uncertainty of 1%.

7.4. PMT nonlinearity

The uncertainty is evaluated by applying half the magnitude of the nonlin-
395 earity reference curve to recalculate the reconstructed energy of MC on a strip
by strip basis. It has a large effect for rare high activity strips, but for hadronic
tracks and showers at these low energies the overall effect is modest. This effect
is one way, there is no PMT nonlinearity in the simulation, so it serves only
to move the simulated energy lower, or could alternately be use as a correction
400 that would be used to move the energy in the data higher.

7.5. Event selection

The proton sample does not pick up a significant uncertainty from this,
except for the data point at $KE = 0.15$ GeV where there is a significant pion
background. The pion sample selection intrinsically allows in an electron and
405 kaon background. Modest variations in those selections yield a 0.7% uncertainty
for π^+ and twice the uncertainty for π^- .

7.6. Energy scale

The absolute energy scale is dominated by the material model for the scin-
tillator planes and affects both data and MC. The calibration procedure uses a
410 comparison of simulated cosmic ray muons to measured muons, so by construc-
tion the data/MC relative energy scale is very well constrained. The largest

contribution to this relative uncertainty comes from observations of discrepancies between the TE and EH data sets, and not from the design of the method or the statistics of the data samples. Within each subsample, there is no discern-
415 able time dependent trend that would extrapolate between these two detector configuration. The uncertainty listed here is taken to be half the discrepancy seen in the muon calibrations between the TE and EH data sets.

7.7. *Cross talk*

A measurement of the cross talk in the cosmic muon calibration finds it con-
420 tributes an average of $4.2 \pm 0.5\%$ to the energy in the detector, and the amount in the MC is tuned to reproduce this. Because the energy calibration of the detector specifically does not include cross talk, this amount is subtracted from the total, and the remaining 0.5% uncertainty contributes to the calorimetric uncertainty between data and MC. Analysis of neutrino data also has cross talk
425 in the simulation tuned to the data, and uses multiple techniques to deal with cross talk; thresholds, topological identification, and subtraction depending on the analysis.

7.8. *Absolute energy scale*

There are additional effects which apply equally to both data and MC ab-
430 solute energy scale, and enhance that beyond to the relative energy scale uncertainties. The most important ones come from the material model for the scintillator planes, and also the lead and steel absorber. They affect both the calibration of the energy deposits in the detector as well as how deep the hadronic activity propagate into the detector. They add an additional 2% in quadrature
435 to the quantities above.

7.9. *Geant4 step size*

The simulation is affected by a number of different Geant4 settings, including some that are unrelated to the hadronic physics model. An interesting one is the fidelity obtained with the default Geant4 adaptive step size algorithm

440 for stepping particles through the simulated detector, subject to certain user
specified maximum steps. Purposely making the maximum step size 0.05 mm
allows the adaptive algorithm to still choose smaller steps near material bound-
aries but never larger steps. This change results in a reduced MC response of
1% for pions and no effect for 0.5 GeV/c electrons. This is consistent with
445 triggering an enhanced Birks' effect because now the simulation is producing
more highly quenched energy deposits. The simulation here uses essentially the
default settings, the same as used for the full MINERvA, so all the calibrations
and measurements are done with a consistent set of parameters, and there is no
uncertainty to assign.

450 7.10. PMT afterpulsing

[This subsection is likely to be removed or more carefully worded. It re-
mains here temporarily.] Another variation in the event selection cuts events
when additional substantial activity is reconstructed within 800 ns following the
triggered event. The response in the MC, which has neither pileup nor after-
455 pulsing simulated, rises because of the correlation with neutrons, electrons from
 π to μ to e decay, and other delayed activity that correlates with systematically
low energy response. However, the response for the data falls slightly and ends
about 1% below where the MC predicts. Pileup triggers removed with this cut
should be uncorrelated with the energy of the triggered event, but large shower
460 data events generate more afterpulsing and are more likely to have afterpulsing
activity reconstructed as another event in this 800 ns window. Because the
default analysis does not make a tight cut on this time window, this is not an
uncertainty. Instead, its the confirmation that these unsimulated properties of
the real experiment are safely negligible.

465 8. Pion calorimetry

There are pion samples with two polarities. The EH π^+ sample was obtained
concurrently with the proton sample while the π^- sample was from the data set

taken the previous week. After these data were taken, the detector configuration was changed to the TE configuration, but unlike for protons, containment in the TE is not adequate for a pion calorimetry measurement. Another difference is that the lowest beam momenta available cause the lowest pion energy for this analysis to be 0.35 GeV, just above the Δ production peak, so very few pions stop at the end of their range in the detector.

The event selection and energy measurement proceed similar to the proton case, correcting the observed energy for passive material, cross talk, and the last-four-plane veto. The denominator for the response for pions is taken to be the total energy. For pions there is a potential background at low energy from electron contamination which is neither simulated nor subtracted but is evaluated to be a small uncertainty.

The MC describes the response to pions well, but not perfectly, and is shown in Fig. 8. The statistical uncertainty on the data is shown while the same for the MC is negligible, and all systematic uncertainties (with their energy dependence) from Table 1 are incorporated into the MC error band. One way to characterize the agreement is the MC models the single particle response within 3% at these energies.

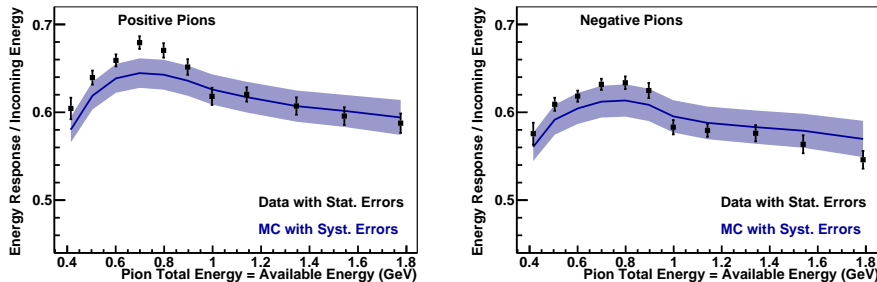


Figure 8: Calorimetric response for positive (left) and negative (right) pions. The errors on the data are statistical only, while the error band on the MC represents the systematic uncertainties on comparisons between data and MC, while a larger uncertainty of up to 4.2% applies to the absolute response scale both data and MC.

While the MC error band is near or touching the data points' statistical

error bars, the MC does not accurately model a change in behavior that starts at 0.9 GeV. This change correlates with a mild trend to flattening out the MC response, and the onset and the magnitude of the discrepancy are the same for
490 both π^+ and π^- , equivalent to a -5% change from low to high energy relative to the MC. The experimental systematic uncertainties permit some motion, especially the beamline systematics, species and pileup backgrounds, and are evaluated could produce a $\pm XYZ\%$ change over this energy range. Instead of taking an overall uncertainty in the response, a MINERvA neutrino analysis
495 sensitive to this trend can propagate this trend instead.

In principle, these data are a test of our ability to model the detector itself as well as the reaction and energy loss processes for pions. We have investigated the sensitivity to model uncertainties in how interactions proceed to inelastic, pion absorption, and elastic fates in the Bertini Cascade model [10] within
500 Geant4, including consideration of pion cross section data [11, 12]. However, calorimetry is more sensitive to the total available energy than it is to differences in outcome for any of these individual fates. Trial 30% modifications to the relative mix of fates have at most 0.5% effect on calorimetry. More important is the magnitude of the reaction cross section or the mean free path in the
505 detector before these fates occur. In this geometry, changes of $XYZ\%$ can have 2% effects on calorimetry. Uncertainties on the models in Geant4 in principle could be energy dependent.

The π^+/π^- ratio cancels a number of common systematics, including the trend in the preceding paragraph. The MC predicts that π^+ yield a 4.8% higher
510 response than π^- , the measured ratio is 6.2%, consistent with flat across this energy spectrum for both. The statistical uncertainty in the data ratio is only 0.5% averaged over these energies. The 0.6% uncertainty in the energy scale comes primarily from an unknown time or detector configuration dependent effect, which should conservatively be applied to this ratio. There is no evi-
515 dence for either an intensity effect (the π^+ data was at higher intensity) or an operational effect due to time or polarity in the beamline, nor a temperature effect, judged by comparing two halves of each data configuration further split

along these operational parameters, though these tests are themselves afflicted by 0.7% statistical uncertainty. This discrepancy is at two standard deviations, and can be used if a situation arises where a conservative uncertainty on the ratio is needed.

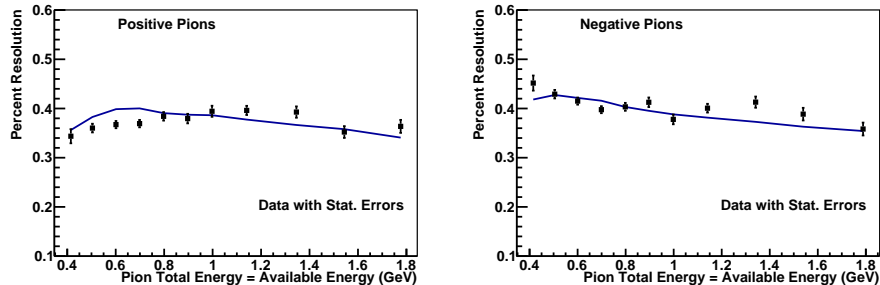


Figure 9: Resolution of the calorimetric response for positive (left) and negative (right) pions. The statistical error on the RMS is shown for the data, no systematic uncertainties are included.

For neutrino experiments, having accurately modeled resolution is also important. Many neutrino distributions are strongly peaked in reconstructed energy or some other kinematic quantity, and an error in resolution will flatten or sharpen the MC peak relative to the data, causing a bias in unfolded distributions and fit parameters. The pion response resolution, shown in Fig. 9, is well modeled. [Rik notes, the sentiment in this paragraph should go with the earlier proton version.]

9. Electron calorimetry

The production and acceptance of electrons in the tertiary beam used for the 2010 MINERvA test beam data limits the electron sample to energies in a range from 0.4 to 0.5 GeV. Using the EH detector configuration, these electrons begin and complete >95% their electromagnetic shower in the ECAL portion of the detector, and the detector response in this special case can be isolated.

The electron sample is separated from the pion sample using a combination

of topological and time-of-flight selections. Events that resemble late-interacting pions because they are tracked into the HCAL or because they have a substantial fraction of energy in the back half of the detector are rejected. Further, the number of strips recording activity is systematically more for electrons, and the variance in energy per plane for EM showers is much higher than for interacting pions. Using the MC, we estimate the efficiency for selecting electrons (pions) to be 73% (8%) for the EH configuration. The pion and electron peaks separate in time of flight by at least 0.7 ns at 0.5 GeV, well within the 0.2 ns resolution of the TOF. Extrapolating the pion distribution just above the TOF cut into the selected electron region in data yields an estimate of one pion background in 50 electron events. An eye-scan of the resulting events with the website-based MINERvA event display [7] confirms there is negligible background.

The data and MC for electrons and positrons for the EH configuration were combined into one sample. The resulting sample is analyzed similarly as previously described for protons and pions. After correcting for passive material, cross-talk, and pileup background activity, the response ratio is obtained for every event. The electron response fraction is found to be 0.776 ± 0.018 (statistical) in data and 0.740 ± 0.002 (statistical) in MC. There is a ± 0.012 relative systematic uncertainty between the data and MC for this fractional response (1.5%) and adding the material assay this becomes a 2.2% absolute uncertainty. The data response is 5% higher than the MC predicts, about twice the 2.8% total uncorrelated uncertainty. The MC predicts the response in the TE configuration is 3% higher, because most electrons ionize their way through the tracker before electromagnetic showers develop in the ECAL. The same 5% excess response is seen in the TE results.

This sample is subject to the same systematics as the proton and pion results plus additional uncertainties due to the electron-pure selection. Comparing the default MC to a variation with $\pm 1.2\%$ Pb density in the ECAL reveals only a $\pm 0.15\%$ change in response for the TE configuration and $\pm 0.3\%$ change for the EH sample. Variations of the event selection contributes 1% uncertainty to the response. The absolute energy scale uncertainty is the same 1.5% and the

data vs. MC relative uncertainty is 0.7%, from the material model effects and calibrations described previously, plus another 0.5% from the cross talk model. Finally, the beam momentum uncertainty is 1% at these energies.

570 For some neutrino analyses, especially with electron or neutral pion final states, the accuracy of the electromagnetic response is of interest. For high energy hadronic showers, it is traditional to form the e/π response ratio. A shower initiated by a charged hadron will typically have both hadronic and electromagnetic components, the relative fractions of each evolve with energy
575 and vary stochastically event by event. An e/π response calibration illustrates the accuracy of these components separately. In the case of this detector, the comparison of 0.8 for electrons to 0.6 for pions provides a helpful rule of thumb. A detailed comparison of the ratio to the one predicted by the MC does not yield a clean interpretation because these two samples are too unique in multiple
580 and uncorrelated ways.

10. Tracking validation

The proton sample in the TE detector configuration allows us to validate proton tracking efficiency, the probability that a proton will be reconstructed as a three-dimensional track object. This proton tracking efficiency, and also
585 for pions, is an important correction used for analysis of neutrino cross sections with specific proton and pion final states.

The sample is similar to the one used for the Birks' parameter measurement where protons stop not later than plane 19, but without the requirement that its depth be consistent with a proton at the end of its range. Another difference,
590 the sample is extended earlier to protons whose last activity is plane 6. This tests a combination of the standard MINERvA "long tracker" which requires a minimum of 11 planes and two variations of the short tracker which under ideal circumstances can form tracks with as few as five planes. For this analysis, the MC sample is four times the size of the data sample. The range of angles with
595 respect to the detector axis is $XY \pm Z$ degrees.

For this sample, protons with kinetic energy less than 0.4 GeV whose last energy deposit is between planes 9 and 19 (inclusive) are tracked with efficiency of $99.2^{+0.2}_{-0.3}\%$ in data and $99.8\pm 0.1\%$ in MC. For the data, this corresponds to tracking 1520 out of 1533 protons in the sample and the binomial error so close
600 to perfect that the uncertainty is asymmetric. This sample has around 60% of protons stopping a distance consistent with the end of their range, and failing the tracking is highly correlated with a proton experiencing an interaction.

Differences begin to appear for even shorter proton samples. For the 185 protons that appear to stop in plane 8, 178 of them were tracked, which gives
605 $96.2^{+1.2}_{-1.6}\%$ compared to the MC $97.7^{+0.5}_{-0.6}\%$. For protons that appear to stop in planes 6 and 7 only 308 out of 338 are tracked, $91.1^{+1.5}_{-1.6}\%$ compared to the MC $96.5\pm 0.5\%$. These subsamples have a 70% fraction consistent with stopping at the end of their range, and its more likely in the data that a short event at the end of its expected range will not pass the tracking requirements.

The above results were obtained with a short tracker configured for a neu-
610 trino pion production analysis [5] (but here applied to the proton sample). A somewhat different configuration optimized for a quasi-elastic proton analysis [6] gives slightly higher efficiency, successfully tracking an additional 6, 1, and 8 events in the data subsamples for the shortest, 8-plane, and longest samples
615 respectively, with a similar trend to tracking more in the MC.

[Need a discussion, what did we learn about the mechanism for tracking failures? sensitivity to gaps ?]

These results suggest that tracking efficiency is adequately modeled (within 1%) for tracks greater than 9 planes, which makes it a negligible uncertainty
620 for neutrino analyses. In contrast, we can use a data-based correction to the efficiency for shorter track lengths of as much as 5%, relative to the MC predicted efficiency. Because the tracking algorithm also has to deal with activity near the neutrino interaction point and wider range of angles relative to the detector axis, but not in the test beam sample, this efficiency correction should be on top
625 of the MC prediction for efficiency considering all effects seen in real neutrino interactions.

[Is there a number from Brandon or Tammy’s analysis that gives an interesting comparison to this 5% number? This correction of 5% is smaller ? of the same size ? as the typical Geant4 uncertainties in the probability to interact?]

630 **11. Muons**

[There is a new problem with muons delta and brem in the main detector. We also have muon data in test beam. Not sure if MEU tuning folks issued a warning that muon clusters were poorly modeled, and the brem delta activity should be in the high side tail of the calibration distributions away from where
635 the peak fit is done.

A fast moving analysis team could pull this from the cosmic ray or beam-muon data, and someone can check Geant4 for muon simulation options that we have incorrectly chosen. If we can’t quickly rule out cross talk and noise, we might have an easy way to quantify the discrepancy suitable for this NIM, the
640 bar is not so high, I think. On the other hand, we probably don’t have that kind of effort, and we’ll remove this suggestion from the draft.

12. Conclusion

We have measured the performance of the tracking and calorimetry of the MINERvA detector design by exposing a miniature version test beam detector
645 to a test beam of low momentum protons, pions, and electrons from the Fermilab Test Beam Facility. These data provide a constraint on the Birks’ law saturation effect for our formulation of polystyrene based plastic scintillator. The calorimetric response to protons and pions within the range of energies tested yields uncertainties of 3% to be applied when the single particle response is used in
650 neutrino analyses. The electron sample yields a larger uncertainty. Tracking performance is well modeled, and we have measured a small discrepancy between the performance of tracking in the data and simulation. In summary, there are several effects that could be interpreted as 2σ fluctuations relative to the systematic uncertainties, while overall the MC describes the data well.

655 **Pseudoreferences**

To do: literature search for other calorimetry results near this range.

C. Adloff et al [Calice] arXiv 1207.4210 probably in NIM or the european version, its modern but higher energy.

I think there is very little calorimetry to be found that is similar enough to what we are doing. There are some references for Birks parameter estimations to add.

References

- [1] L. Aliaga, et al., Design, Calibration, and Performance of the MINERvA Detector, Nucl.Instrum.Meth. A743 (2014) 130–159. arXiv:1305.5199, doi:10.1016/j.nima.2013.12.053.
- [2] L. Fields, J. Chvojka, et al., Measurement of Muon Antineutrino Quasi-Elastic Scattering on a Hydrocarbon Target at $E_\nu \sim 3.5$ GeV, Phys. Rev. Lett. 111, 022501. arXiv:1305.2234, doi:10.1103/PhysRevLett.111.022501.
- [3] G. Fiorentini, D. Schmitz, P. Rodriguez, et al., Measurement of Muon Neutrino Quasi-Elastic Scattering on a Hydrocarbon Target at $E_\nu \sim 3.5$ GeV, Phys. Rev. Lett. 111, 022502. arXiv:1305.2243, doi:10.1103/PhysRevLett.111.022502.
- [4] B. Tice, M. Datta, J. Mousseau, et al., Measurement Ratios of ν_μ Charged-Current Cross Sections on C, Fe, and Pb to CH at Neutrino Energies 2–20 GeV, Phys. Rev. Lett. 112, 231801. arXiv:1403.2103, doi:10.1103/PhysRevLett.112.231801.
- [5] B. Eberly, et al., Charged Pion Production in ν_μ Interactions on Hydrocarbon at $\langle E_\nu \rangle = 4.0$ GeV arXiv:1406.6415.
- [6] T. Walton, et al., Measurement of muon plus proton final states in ν_μ Interactions on Hydrocarbon at $\langle E_\nu \rangle = 4.2$ GeV arXiv:1409.4497.

- [7] N. Tagg, et al., Arachne - A web-based event viewer for MINERvA, Nucl.Instrum.Meth. 676 (2012) 44–49. [arXiv:1111.5315](#), [doi:10.1016/j.nima.2012.01.059](#).
- 685 [8] S. Agostinelli, et al., GEANT4: A Simulation toolkit, Nucl.Instrum.Meth. A506 (2003) 250–303. [doi:10.1016/S0168-9002\(03\)01368-8](#).
- [9] J. Allison, K. Amako, J. Apostolakis, H. Araujo, P. Dubois, et al., Geant4 developments and applications, IEEE Trans.Nucl.Sci. 53 (2006) 270. [doi:10.1109/TNS.2006.869826](#).
- 690 [10] A. Heikkinen, N. Stepanov, J. P. Wellisch, Bertini intranuclear cascade implementation in GEANT4, eConf C0303241 (2003) MOMT008. [arXiv:nucl-th/0306008](#).
- [11] D. Ashery, I. Navon, G. Azuelos, H. Walter, H. Pfeiffer, et al., True Absorption and Scattering of Pions on Nuclei, Phys.Rev. C23 (1981) 2173–2185. [doi:10.1103/PhysRevC.23.2173](#).
- 695 [12] B. Allardyce, C. Batty, D. Baugh, E. Friedman, G. Heymann, et al., Pion reaction cross-sections and nuclear sizes, Nucl.Phys. A209 (1973) 1–51. [doi:10.1016/0375-9474\(73\)90049-3](#).